Biedermann, N., Winkler, B., Speziale, S., Reichmann, H.-J., Koch-Müller, M. (2017): Single-crystal elasticity of SrCO3 by Brillouin spectroscopy. - *High Pressure Research*, *37*, 2, pp. 181—192.

DOI: http://doi.org/10.1080/08957959.2017.1289193

Single-crystal elasticity of $SrCO_3$ by Brillouin spectroscopy

N. Biedermann[1], B. Winkler[2], S. Speziale[1], H. J. Reichmann[1], M. Koch-Müller[1]

[1]*GFZ German Research Center for Geosciences, Potsdam, Germany*
[2]*Institute for Geosciences, Goethe University Frankfurt, Frankfurt am Main, Germany*

Abstract

The elastic stiffness tensor c_{ij} of synthetic strontianite ($SrCO_3$) was determined by Brillouin spectroscopy at ambient conditions. An inversion procedure based on Christoffel's equation was used to determine the 9 independent elastic coefficients of orthorhombic strontianite from acoustic velocities measured along 69 different crystallographic directions in 3 randomly oriented crystal platelets. The best fit values of c_{11}, c_{12}, c_{13}, c_{22}, c_{23}, c_{33}, c_{44}, c_{55} and c_{66} are 153(1), 52(1), 38(11), 109.6(8), 43(15), 75(1), 28.0(5), 28.6(4) and 33.2(5) GPa, respectively. The linear compressibilities of *a*-, *b*- and *c*-axis at ambient conditions are 3(2), 4(6) and 10(8) $\cdot$ 10^{-3} GPa^{-1}. The adiabatic bulk modulus of strontianite is 64(4) GPa, intermediate between aragonite ($CaCO_3$) and witherite ($BaCO_3$), thus confirming a systematic linear relationship between cation radius and bulk modulus in aragonite-type carbonates. The shear modulus of strontianite has a value of 31(1) GPa which is about 10 % smaller in comparison to aragonite.

Keywords: Brillouin spectroscopy, strontianite, elasticity, elastic tensor

Corresponding author

N. Biedermann, GFZ German Research Center for Geosciences, Telegrafenberg, 14473 Potsdam, Germany, mail: nicole.biedermann@gfz-potsdam.de, phone: +49 (0)331/288 – 27510

New address (beginning from 1.1.2017): European XFEL, Holzkoppel 4, 22869 Schenefeld, Germany, mail: nicole.biedermann@xfel.eu

This is an Accepted Manuscript of an article published by Taylor & Francis in High Pressure Research on 13.02.2017 available online: http://www.tandfonline.com/ *[DOI: 10.1080/08957959.2017.1289193]*

1. Introduction

Carbonates are among the most important crustal materials. Carbonates are also present in the deep Earth as confirmed by their presence as inclusions in transition-zone diamonds [1]. Thermodynamic calculations suggest that carbonates are stable during subduction and carbon can therefore be reintroduced into the mantle, where it is stored within several phases including diamond, carbonatitic melts and carbonate minerals.

Strontium carbonate ($SrCO_3$) is an important chemical component of natural carbonates and especially of alkali-carbonates formed during mantle evolution [2]. $SrCO_3$ occurs as an independent mineral phase (strontianite) in hydrothermal environments and carbonatites. Strontianite crystallizes in the orthorhombic system and is isostructural to aragonite, the high pressure polymorph of calcite. In order to properly model the thermodynamic properties of dense carbonates at mantle depth we need to have a complete knowledge of the physical properties of the endmember components such as strontium carbonate.

A number of studies have investigated the thermo-elastic properties of calcite-structured carbonates [3–10]. In contrast, the elasticity of aragonite-group minerals has been investigated only in two experimental studies of natural aragonite: Voigt [11], who determined the elastic coefficients with ultrasonic interferometry and Liu et al. [12], who measured the elastic coefficients with Brillouin spectroscopy. Recently, all tensor components of $SrCO_3$ have been predicted based on density functional theory, DFT, calculations [13]. The study of Nguyen-Thanh et al. [13] was complemented with high resolution inelastic x-ray scattering experiments to obtain the c_{33} tensor component. However, without further experimental data these results cannot be benchmarked against experiment. In this study we present the first experimental data set for the elastic stiffness tensor of pure $SrCO_3$ at ambient conditions. These new results present a reference required for the evaluation of the effects of chemical substitution and the influence of pressure and temperature on the elastic properties of aragonite-type minerals can be established.

2. Samples and Methodology

Sample material

Pure strontianite crystals ($SrCO_3$) were synthesized at 4 GPa and 1273 K for 24 hours in a Walker-type multi-anvil module [14]. $SrCO_3$ powder from sigma Aldrich Chemical Company (99.995% purity) was used as a starting material. We intentionally did not remove traces of adsorbed water in the starting material as this may have served as a flux to enhance the growth of large crystals and indeed we recovered single crystals of $SrCO_3$ up to 500 µm in size (Fig. 1). Grains of various sizes were ground and polished from both sides with SiC paper (final grain size of 5 µm) in order to obtain face-parallel platelets for Brillouin scattering measurements. Three platelets of suitable size and surface quality with random orientation (*$SrCO_3$_1*, *$SrCO_3$_2*, *$SrCO_3$_3*) with diameter > 200 µm and thickness between 50 and 80 µm were chosen for the investigations. The platelets were optically transparent and colourless. Due to the difficulty in preparing the sample platelets we decided to determine their orientation only after measuring Brillouin scattering. However, two of the three platelets were damaged when removed from the sample holder after the Brillouin experiments. The orientation of platelet *$SrCO_3$_3* was determined by electron backscattered diffraction (EBSD) as (0 0.67 1). The orientations of platelet *$SrCO_3$_1* and *$SrCO_3$_2* could be precisely determined during the inversion of Brillouin scattering results [15] and are (0.22 -0.5 1) and (-0.35 0.35 1).

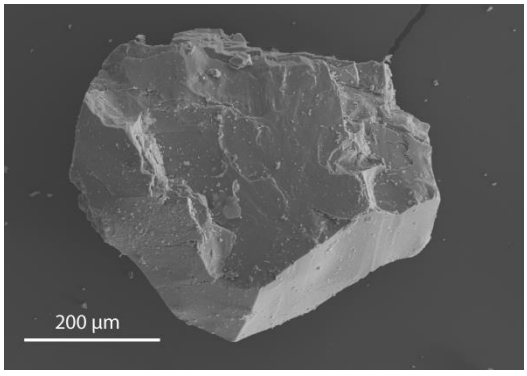

Fig. 1: SEM image of a synthetic $SrCO_3$ crystal.

X-ray diffraction

We performed powder X-ray diffraction measurements at ambient conditions and in transmission mode using a fully automated STOE Stadi P diffractometer, equipped with a primary monochromator and a 7° wide position sensitive detector. Standard operating conditions ($CuK\alpha_1$-radiation, 40 kV and 40 mA) were used for data collection in the 2Θ range 5-125° in 0.1°intervals. For structure refinements Rietveld analyses were performed using the GSAS software package [16].

Brillouin spectroscopy

Brillouin scattering is the inelastic scattering of light on acoustic phonons. The process produces scattered light with both, higher or lower frequency than the incident light. A typical Brillouin spectrum produced by an elastically anisotropic solid consists of one strong elastically scattered signal (Rayleigh peak) and three pairs of peaks corresponding to the three polarizations of the scattering acoustic phonons (Fig. 2). Each of them has a different frequency shift $\Delta\omega$ with respect to the incident beam, that is: one longitudinal mode (L) that is associated with displacement in the direction of propagation and two transverse modes (T1 and T2) with displacement perpendicular to the propagation direction (e.g [17]). The geometry of the experiment defines the scattering angle, which is directly related to the scattering wave vector q. The frequency shift of each mode $\Delta\omega$ is converted into velocity (v) of the acoustic waves through the material as $v = \Delta\omega/q$.

A set of velocities of compressional waves and shear waves measured in different crystallographic directions are used to constrain the full set of elastic coefficient c_{ij} by inversion of the Christoffel's equation [18]:

$$\left|\left(c_{ijkl} * q_i * q_j - \rho v^2 * \delta_{lk}\right)u_k = 0\right| \quad \text{(Eq. 1)}$$

where $q_{i/j}$ are the scattering wave vectors, u_k is the displacement vector, ρ is the density, v are the measured acoustic velocities and δ_{lk} is the Kronecker delta. The isotropic aggregate adiabatic bulk modulus K_s and the shear modulus G of the material are then calculated from the set of c_{ij} coefficients.

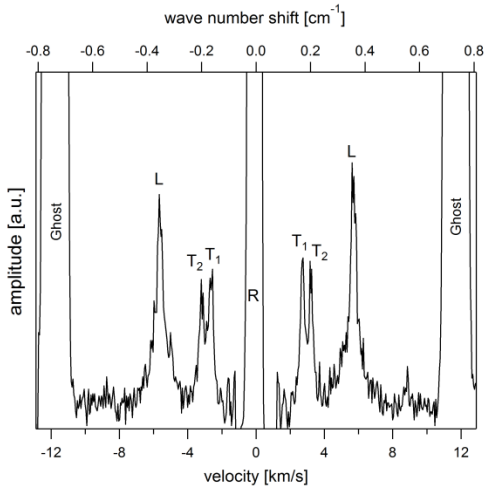

Fig. 2: A representative Brillouin spectrum of $SrCO_3$ in one general direction of propagation within the crystal and with one longitudinal acoustic mode (L) and two transverse acoustic modes (T1 and T2). R: Rayleigh peak

Brillouin scattering measurements were performed in the Brillouin scattering laboratory at the German Research Centre for Geosciences GFZ in Potsdam. The Brillouin setup is based on a tandem Fabry-Perot spectrometer [19]. The light source is a solid-state laser ($Nd:YVO_4$) which produces a monochromatic green light with a wavelength of 532 nm. The total power focused on the sample was between 30 to 80 mW, depending on the probed crystallographic direction. Scattered Brillouin signal was collected in a symmetric forward scattering geometry with an external angle (θ) between incident beam and scattered light of 60° and then frequency-analyzed by a six-pass tandem Fabry-Pérot interferometer. This scattering geometry, in which the sample's interfaces are perpendicular to the bisector of θ, allows the determination of the acoustic velocities (v) without knowing the refractive index of the material [20]:

$$v = \frac{\Delta\omega * \lambda_0}{2 * \sin\left(\frac{\theta}{2}\right)} = \Delta\omega * \lambda \quad \text{for } \theta = 60° \qquad \text{(Eq. 2)}$$

with $\Delta\omega$ as the measured Brillouin frequency and λ_0 and λ as the wavelength of the unshifted incident laser beam in air and in the sample, respectively. The scattered light was detected with a photomultiplier tube. The platelets were placed into a sample holder between two polycrystalline diamond windows whereas one of the sample's surfaces is in contact with a diamond plate [21]. The holder was mounted on

an Eulerian cradle and spectra were collected at a rotational angle from 0 to 180° at regular intervals of 5° (*SrCO$_3$_2*), 10° (*SrCO$_3$_3*) or 15° (*SrCO$_3$_1*) azimuthal angle beginning from one general direction.

DFT calculations

DFT calculations were performed with commercial and academic versions of the CASTEP program [22] using a generalized gradient approximation formalized by Wu and Cohen [23] with a plane wave basis set and qc-optimized norm-conserving pseudopotentials [24] or "on the fly" pseudopotentials from the CASTEP data base. The maximum cutoff energy of the plane waves was 900 eV. An 8 x 4 x 6 Monkhorst–Pack grid [25] was employed for sampling of reciprocal space, corresponding to a k-point separation of less than 0.030 Å^{-1}. Elastic stiffness coefficients were obtained from stress-strain relations [26]. Full geometry optimisations were carried out until forces were smaller than 0.01 eV/Å and no component of the stress tensor exceeded 0.02 GPa. The accuracy of this approach has previously been established by comparison of computed structural and physical parameters at ambient pressure to experimental data [13].

3. Results

Results from powder X-ray diffraction show lattice parameters with a = 5.1029(7) Å, b = 8.4075(1) Å, c = 6.0229(1) Å and a measured density of 3.795 g/cm³. These lattice parameters are in excellent agreement with published data for strontianite [27]. More than 120 acoustic velocity data were collected from the three samples along a total of 69 distinct directions. Most of the Brillouin spectra show strong intensities for compressional wave velocities (v_p) with high signal-to-noise ratios. The intensities for the shear wave velocities (v_{s1} and v_{s2}) are weaker in a number of directions and in some cases no signal for v_s was observed. To improve the signal of v_s the spectrometer acquisition setting was modified in order to increase the measuring time by a factor of 10. As shown in Fig. 3, a pronounced anisotropy for the acoustic velocities is visible.

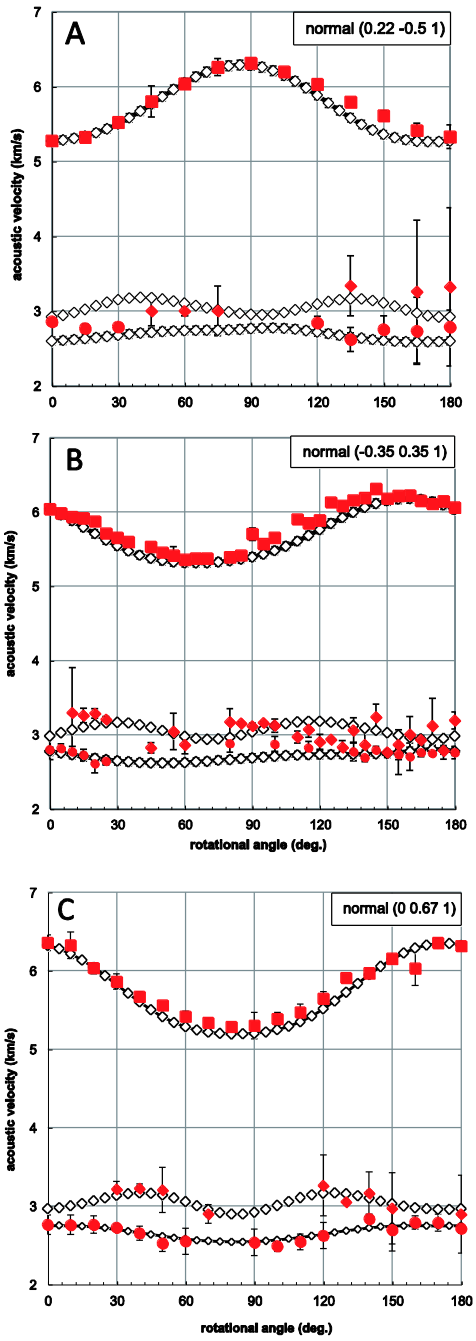

Fig. 3 a-c: Observed longitudinal (red filled squares) and transverse (red filled circles) modes of $SrCO_3$ as a function of rotational angle. Calculated velocities are marked with solid lines and open squares.

Strontianite has an orthorhombic crystal structure with space group P*mcn* [28]. Hence, the elastic stiffness tensor c_{ij} has 9 independent non-zero tensor components which are c_{11}, c_{12}, c_{13}, c_{22}, c_{23}, c_{33}, c_{44}, c_{55} and c_{66} in contracted Voigt notation. The complete velocity data set was used to determine the coefficients of the elastic tensor. The inversion procedure was performed fixing the Eulerian angles (which

describe the relationship between crystalline and experimental reference systems) for the platelet *SrCO$_3$_3* and refining those of platelet *SrCO$_3$_1* and *SrCO$_3$_2* (see e.g. [29]). Due to the orientation of the three platelets, our dataset of Brillouin scattering measurements lacks measurements in directions belonging to (100) and (010) crystallographic planes. This limits the constraints on the coefficients c_{13}, c_{23} and c_{33}. In order to reduce the uncertainties on these constants we added to the original Brillouin dataset the results of IXS measurements [13] of the longitudinal acoustic phonon dispersion curve in the crystallographic z-direction, which constrain the coefficient c_{33}. However, the uncertainties for c_{13} and c_{23} are substantially higher than for the other coefficients. The fitted full set of elastic coefficients is reported in Table 1, where we compare our results with the elastic coefficients of $SrCO_3$ derived from DFT calculations and with other carbonates that were determined experimentally.

4. Discussion

Acoustic velocity anisotropy

The investigation of the elastic properties of carbonates, including the elastic anisotropy, at high pressures and temperatures is necessary in order to understand the effect of their presence at great depths in the mantle. However, the elastic properties of complex carbonates also at ambient conditions are poorly documented by experimental studies, with the exception of calcite.

The v_p anisotropy can be analyzed using the anisotropy factor A_p [30] which is defined as:

$$A_p[\%] = \frac{2(v_{p,max} - v_{p,\min})}{(v_{p,max} + v_{p,min})} * 100 \qquad \text{(Eq. 3)}$$

with $v_{p,max} = \sqrt{\frac{c_{11}}{\rho}}$ and $v_{p,min} = \sqrt{\frac{c_{33}}{\rho}}$

where $v_{p,max}$ and $v_{p,min}$ represent the maximum and minimum compressional wave velocities calculated from the fitted elastic coefficients in longitudinal direction. The polarization anisotropy factor for the shear wave velocities A_s can be described as (e.g. [30]) :

$$A_s[\%] = \frac{(v_{s1} - v_{s2})}{v_s} * 100 \qquad \text{(Eq. 4)}$$

$$\text{with} \qquad v_s = \sqrt{\frac{G}{\rho}}$$

and defines the difference in percentage between the velocities of the two orthogonally polarized S-waves (v_{s1} and v_{s2}) in a given direction normalized to the average shear wave velocity v_s. As shown in Nguyen-Thanh et al. [13], the highest shear wave velocity anisotropy $A_{s,max}$ in $SrCO_3$ is found in direction (111) with 18.2 % calculated from our experimental data. Their DFT calculations are in perfect agreement with our fitted elastic coefficients. However, differences up to 19% are found in the coefficients c_{44} and c_{66} thus lowering the experimentally determined maximum polarization anisotropy factor $A_{s,max}$ significantly with respect to the theoretical value.

A better quantification of the single-crystal anisotropy is given by the universal anisotropy index A^u [31] in which the full tensorial character of the elastic stiffness is used:

$$A^u = 5\frac{G_V}{G_R} + \frac{K_V}{K_R} - 6 \qquad \text{(Eq. 5)}$$

K_V and G_V are the Voigt bounds of the bulk and shear modulus, respectively, and K_R and G_R are the Reuss bounds. Table 1 shows the universal anisotropy index A^u for selected carbonates. In the case of magnesite, which seems to be the most stable carbonate at lower mantle conditions [32–34], the universal anisotropy index A^u is significantly higher compared to the aragonite-type carbonates. The rhombohedral structure of magnesite at ambient conditions is less dense than the orthorhombic phase of strontianite and results in a much larger anisotropy for the seismic wave velocities. In addition, Yang et al. [8] reported that the anisotropy for magnesite increases with depth and that the high velocity anisotropy of carbonates can be used to detect carbonatitic regions in the lower mantle. Strontianite, as a component in complex carbonates, can lower the anisotropy.

The elastic tensor c_{ij} of $SrCO_3$

Different elastic moduli calculated from the best fit elastic coefficients of strontianite are presented in Table 1 together with previously published data for aragonite measured by Brillouin spectroscopy [12]. If we compare the elastic coefficients of $SrCO_3$ with that of aragonite ($CaCO_3$) both structures display an order of $c_{11} > c_{22} > c_{33}$ and $c_{11} > c_{12} > c_{13}$ but with significantly lower values for c_{11} and c_{33} in $SrCO_3$. Weakening of the longitudinal elastic coefficients related due to the larger ionic radius for Sr^{2+} compared to Ca^{2+} is also observed in the simple oxides SrO and CaO [35–37]. In detail, the x-crystallographic direction is 12% softer than in aragonite under uniaxial stress. The z-crystallographic direction which is perpendicular to the CO_3 planar groups is 25 % less stiff than in $CaCO_3$. The off-diagonal elastic coefficients c_{12}, c_{13} and c_{23} are approximately equal in both phases indicating a lower dependence on the cation size. It is worth mentioning that the aragonite sample used by Liu et al. [12] contains some significant amount of Sr^{2+} (2.5 mol%).

The Voigt-Reuss-Hill average for the aggregate bulk modulus K_{VRH} of $SrCO_3$ derived from our results is 64(4) GPa and is in perfect agreement with the computational study of Nguyen-Thanh et al. [13] which reports a bulk modulus of 63(3) GPa. Our aggregate moduli are shown in Table 2 together with previously published data for $SrCO_3$ obtained by high-pressure X-ray diffraction by Wang et al. [38]. The shear modulus G_{VRH} of $SrCO_3$ has a value of 31(1) GPa which is about 10 % smaller in comparison to that of aragonite (35.8(2) GPa, [12]).

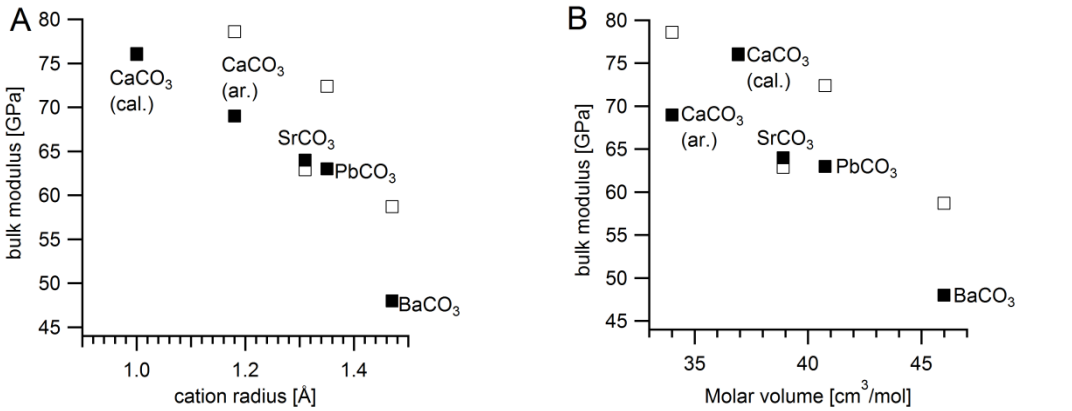

Fig. 4: Dependence of the bulk modulus on (a) the cation radius and (b) the molar volume of calcite and aragonite-type carbonates. The experimentally observed values from Table 2 are marked with filled squares. Values that are marked with open symbols were calculated**.**

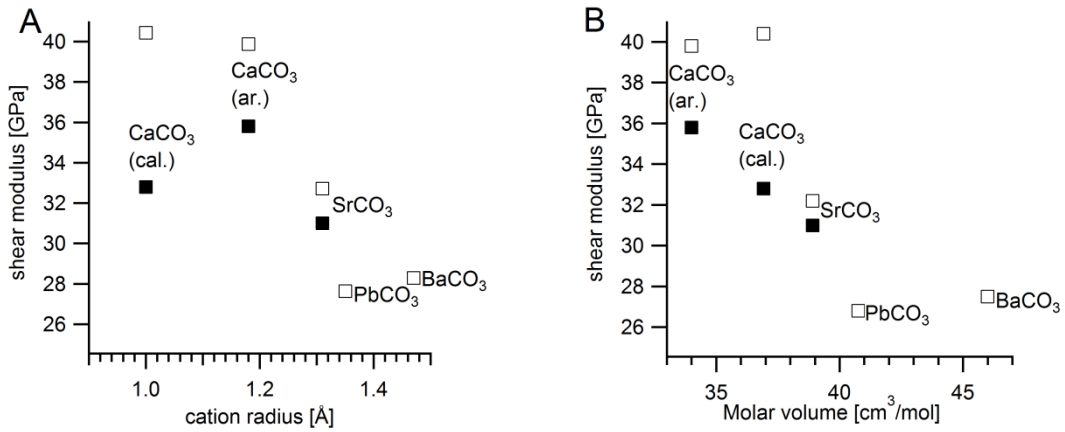

Fig. 5: Shear modulus as a function of (a) cation radius and (b) molar volume for calcite and aragonite-type carbonates. For symbols definition see Fig. 4.

Table 1: Average seismic wave velocities and elastic coefficients of selected carbonates.

	strontianite		aragonite	calcite	magnesite
	This study	**[13]**	**[12]**	**[7]**	**[8]**
C_{11} [GPa]	153 (1)	152 (1)	171.1 ± 1	149.4(7)	260.7 ± 1
C_{22} [GPa]	109.6 (8)	109 (1)	110.1 ± 0.9		
C_{33} [GPa]	75 (1)[1]	74 (1)	98.4 ± 1.2	85.2(18)	157.6 ± 2.6
C_{44} [GPa]	28.0 (5)	34 (1)	39.3 ± 0.6	34.1(5)	57.8 ± 0.4
C_{55} [GPa]	28.6 (4)	26 (1)	24.2 ± 0.4		
C_{66} [GPa]	33.2 (6)	38 (1)	40.2 ± 0.6		
C_{12} [GPa]	52 (1)	54 (1)	60.3 ± 1.0	57.9(11)	74.3 ± 1.5
C_{13} [GPa]	38 (11)	33 (1)	27.8 ± 1.6	53.5(9)	59.7 ± 2.1
C_{23} [GPa]	43 (15)	43 (1)	41.9 ± 2.0		
V_p [km/s]	5.3 (3)	5.3 (3)			8.28 ± 0.04
V_s [km/s]	2.8 (1)	2.9 (1)			4.82 ± 0.02
V_p/V_s	2.0	1.85			1.725
A_p [%]	35.3	35.61	29.62	32.38	26.2
A_{smax} [%]	18.2	22.34	25.86	58.92	36.2
A^u	0.6	0.5	0.48	1.6	0.82

[1]derived from IXS measurements [13].

.

A linear dependence of the compressibility on the cation radius and molar volume in (aragonite-type) carbonates can be observed and it reflects the tendency for larger cations to be more compressible (Fig. 4a and Fig. 4b). Using DFT calculated shear moduli for $PbCO_3$ and $BaCO_3$, a similar trend is observed for the relationship between shear modulus G_{VRH}, cation radius and molar volume of the selected carbonates (Fig. 5a and Fig. 5b).

The linear compressibilities along the orthorhombic axes arise from the elastic compliances s_{ij} which are reciprocally related to the coefficients of the stiffness tensor c_{ij} that can be determined by Brillouin spectroscopy [39]:

$$\beta_a = s_{11} + s_{12} + s_{13} \quad \text{(Eq. 6)}$$

$$\beta_b = s_{21} + s_{22} + s_{23} \quad \text{(Eq. 7)}$$

$$\beta_c = s_{31} + s_{32} + s_{33} \quad \text{(Eq. 8)}$$

Calculated linear compressibilities after equations 6 - 8 from our study are given in Table 2. The very large uncertainties on the values of the linear compressibilities of $SrCO_3$ are entirely due to the propagation of the uncertainties on c_{13} and c_{23}. Our results are in qualitative agreement with the linear compressibilities determined by X-ray diffraction in the study of Wang et al. [38] and were additionally confirmed by DFT calculations.

Table 2: Calculated and experimental axial compressibilites (βx = (d(x/x0)/dP) with x = a, b, c) in 10^{-3} GPa^{-1}, bulk modulus and shear modulus (in GPa) for selected carbonates.

	strontianite			aragonite		witherite		cerussite		calcite	
	exp.[a]	*DFT*[a]	*exp [38]*	*exp [12]*	*DFT*[a]	*Exp [38]*	*DFT*[a]	*exp [40]*	*DFT*[a]	*exp [7,10]*	*DFT*[a]
β_a	3 (2)	3.08	2.9 (1)	3.0(2)	2.1	3.6(2)	3.4	0.72(3)%	3.5	2.62(2)	2.9
β_b	4 (6)	3.68	4.3 (2)	4.6(2)	3.6	4.0(3)	4.6	1.78(3)%	4.8	-	-
β_c	10 (8)	10.00	9.8 (3)	7.3(6)	3.9	15.2(6)	8.3	3.26(4)%	5.8	7.94(7)	6.3
K_V	67 (4)	66.3		71.0	80.4		61.7		76.3		79.6
K_R	60.9 (3)	59.6		66.7	76.8		55.8		68.5		72.7
K_{VRH}	64 (4)	62.9	62 (1)	69 (1)	78.6	48(1)	58.7	63(3)	72.4	76.1	76.1
G_V	32 (1)	33.4		37.2	41.5		28.7		27.4		45.7
G_R	29.8 (3)	31.0		34.1	38.2		26.3		26.1		35.1
G_{VRH}	31 (1)	32.2		35.8 (2)	39.8	-	27.5	-	26.8	32.8	40.4

[a]This study.

The highest compressibility is found in direction of the *c*-axis and is in agreement with the crystal structure of $SrCO_3$ where stronger C-O bonds are present in the a,b-plane and weaker M-O bonds are present in direction of the c-axis. The compressibility in c-axis of $10 \cdot 10^{-3}$/GPa is intermediate between aragonite [12] and witherite [38] thus confirming a dependency on the cation radius. Based on our results on strontianite and assuming a linear relationship between the elastic coefficients and the molar fraction of $SrCO_3$ in natural aragonite, we extrapolated data for the axial compressibilities as well as the bulk and shear modulus for pure aragonite. The data are indistinguishable within uncertainties from those of the natural sample measured by Liu et al. [12], indicating that 2.5 mol% of Sr-carbonate component has a minor influence on the elastic constants.

5. Conclusion

Measuring Brillouin scattering along 69 different crystallographic directions in a set of three platelets has allowed us to determine the full set of single-crystal elastic coefficients of $SrCO_3$. A shear modulus of 31(1) GPa and an adiabatic bulk modulus of 64(4) GPa have been obtained. A comparison with the elastic moduli of other aragonite-type carbonates indicates a linear relationship between cation radius and aggregate moduli. Our experimental results generally are consistent with the results of the DFT calculations although there are noticeable discrepancies in some instances, such as for the elastic stiffness coefficients c_{44} and c_{66}. To resolve the origin of these discrepancies, further experimental data are required.

The highest compressibility is found in direction of the *c*-axis, the direction perpendicular to the planar CO_3 groups. $SrCO_3$, similar to other carbonates, shows a strong dependence of the acoustic velocities on the orientation of the sample. The present data permit to incorporate effects of Sr-Ca substitution on the elastic properties and the seismic velocities of natural deep mantle carbonates. We conclude that an admixture of Sr will lead to a lowering anisotropy with increasing Sr-content.

Acknowledgments

We thank all colleagues from GFZ Potsdam who provided insights and fruitful discussions that greatly assisted the research. We also thank our reviewer for thoughtful comments and suggestions. The research presented in this study has been carried out within the scope of the DFG-funded German research unit DFG FOR 2125 “CarboPaT” (Structures, properties and reactions of carbonates at high pressures and temperatures).

References

1 Brenker FE, Vollmer C, Vincze L, Vekemans B, Szymanski A, Janssens K, Szaloki I, Nasdala L, Joswig W, Kaminsky F. Carbonates from the lower part of transition zone or even the lower mantle. Earth. Planet. Sci. Lett. 2007:260,1–9.

2 Shatskiy AF, Litasov KD, Palyanov Y. Phase relations in carbonate systems at pressures and temperatures of lithospheric mantle: Review of experimental data. Russian Geology and Geophysics. 2015:56,113–142.

3 Dandekar DP, Ruoff AL. Temperature Dependence of the Elastic Constants of Calcite between 160° and 300°K. J. Appl. Phys. 1968:39,6004.

4 Dandekar DP. Variation in the Elastic Constants of Calcite with Temperature. J. Appl. Phys. 1968:39,3694.

5 Humbert P, Plique F. Elastic properties of monocrystalline rhombohedral carbonates - Calcite, Magnesite, Dolomite. Comptes Rendus Hebdomadaines des Se ances de l'Academie des Sciences. 1972,391.

6 Zhang J, Reeder RJ. Comparative compressibilities of calcite-structure carbonates: Deviations from empirical relations. Am. Mineral. 1999,861–870.

7 Chen C-c, Lin C-C, Liu L-G, Sinogeikin SV, Bass JD. Letters. Elasticity of single-crystal calcite and rhodochrosite by Brillouin spectroscopy. Am. Mineral. 2001:86,1525–1529.

8 Yang J, Mao Z, Lin J-F, Prakapenka VB. Single-crystal elasticity of the deep-mantle magnesite at high pressure and temperature. Earth. Planet. Sci. Lett. 2014:392,292–299.

9 Sanchez-Valle C, Ghosh S, Rosa AD. Sound velocities of ferromagnesian carbonates and the seismic detection of carbonates in eclogites and the mantle. Geophysical Research Letters. 2011:38.

10 Redfern SAT, Angel RJ. High-pressure behaviour and equation of state of calcite, $CaCO_3$. Contrib Mineral Petrol. 1999:134,102–106.

11 Voigt W. Lehrbuch der Kristallphysik. BG Teubner, Leipzig. 1910.

12 Liu L-G, Chen C-c, Lin C-CL, Yang Y-j. Elasticity of single-crystal aragonite by Brillouin spectroscopy. Phys Chem Min. 2005:32,97–102.

13 Nguyen-Thanh T, Bosak A, Bauer JD, Luchitskaia R, Refson K, Milman V, Winkler B. Lattice dynamics and elasticity of $SrCO_3$. J Appl Crystallogr. 2016:49.

14 Walker D, Carpenter MA, Hitch CM. Some simplifications to multianvil devices for high pressure experiments. Am. Mineral. 1990:75,1020–1028.

15 Castagnede B, Every AG, Sachse W. Numerical simulation of the instabilities associated to the recovery of elastic constants of anisotropic solids from quasi-longitudinal velocities alone. Comptes rendus de l'Académie des sciences. Série 2, Mécanique, Physique, Chimie, Sciences de l'univers, Sciences de la Terre. 1992:314,865–871.

16 Larson and Dreele. 1987 Generalized structure analysis system. Los Alamos National Laboratory Rep. No. LA-UR-86-748, 16.

17 Krishnan RS. Brillouin scattering. The Raman Effect. 1971:1,343–404.

18 Every AG. General closed-form expressions for acoustic waves in elastically anisotropic solids. Physical Review B. 1980:22,1746.

19 Sandercock JR Fabry-perot interferometer. 1980 ,Google Patents, 19.

20 Whitfield CH, Brody EM, Bassett WA. Elastic moduli of NaCl by Brillouin scattering at high pressure in a diamond anvil cell. Rev. Sci. Instrum. 1976:47,942–947.

21 Scholtzová E, Tunega D, Speziale S. Mechanical properties of ettringite and thaumasite—DFT and experimental study. Cem. Concr. Res. 2015:77,9–15.

22 Clark SJ, Segall MD, Pickard CJ, Hasnip PJ, Probert MIJ, Refson K, Payne MC. First principles methods using CASTEP. Z. Kristallogr. - Crystalline Materials. 2005:220,567–570.

23 Wu Z, Cohen RE. More accurate generalized gradient approximation for solids. Phys. Rev. B. 2006:73,235116.

24 Rappe AM, Rabe KM, Kaxiras E, Joannopoulos JD. Optimized pseudo-potentials. Phys. Rev. B. 1990:41,1227.

25 Monkhorst HJ, Pack JD. Special points for Brillouin-zone integrations. Physical Review B. 1976:13,5188.

26 Milman V, Warren MC. Elasticity of hexagonal BeO. Journal of Physics: Condensed Matter. 2001:13,241.

27 Speer JA, Hensley-Dunn ML. Strontianite composition and physical properties. Am. Mineral. 1976:61,1001–1004.

28 De Villiers J. 1971 Crystal structures of aragonite, strontianite and witherite, 28.

29 Jiang F, Speziale S, Duffy TS. Single-crystal elasticity of grossular-and almandine-rich garnets to 11 GPa by Brillouin scattering. J. Geophys. Res: Solid Earth. 2004:109.

30 Mainprice D, Barruol G, Ismail WB. The seismic anisotropy of the Earth's mantle: from single crystal to polycrystal. Geophysical monograph - American Geophysical Union. 2000:117,237–264.

31 Ranganathan SI, Ostoja-Starzewski M. Universal elastic anisotropy index. Phys Rev Lett. 2008:101,55504.

32 Katsura T, Ito E. Melting and subsolidus phase relations in the $MgSiO_3$ - $MgCO_3$ system at high pressures: implications to evolution of the Earth's atmosphere. Earth. Planet. Sci. Lett. 1990:99,110–117.

33 Isshiki M, Irifune T, Hirose K, Ono S, Ohishi Y, Watanuki T, Nishibori E, Takata M, Sakata M. Stability of magnesite and its high-pressure form in the lowermost mantle. Nature. 2004:427,60–63.

34 Thomson AR, Walter MJ, Lord OT, Kohn SC. Experimental determination of melting in the systems enstatite-magnesite and magnesite-calcite from 15 to 80 GPa. Am. Mineral. 2014:99,1544–1554.

35 Chang ZP, Graham EK. Elastic properties of oxides in the NaCl-structure. J. Phys. Chem. Solids. 1977:38,1355–1362.

36 Speziale S, Marquardt H, Duffy TS. Brillouin Scattering and its Application in Geosciences. Reviews in Mineralogy and Geochemistry. 2014:78,543–603.
37 Speziale S, Shieh SR, Duffy TS. High-pressure elasticity of calcium oxide: A comparison between Brillouin spectroscopy and radial X-ray diffraction. J. Geophys. Res: Solid Earth. 2006:111.
38 Wang M, Liu Q, Nie S, Li B, Wu Y, Gao J, Wei X, Wu X. High-pressure phase transitions and compressibilities of aragonite-structure carbonates: $SrCO_3$ and $BaCO_3$. Phys Chem Minerals. 2015:42,517–527.
39 Nye JF. 1985 Physical properties of crystals: their representation by tensors and matrices, 39.
40 Zhang Y-F, Liu J, Qin Z-X, Lin C-L, Xiong L, Li R, Bai L-G. A high-pressure study of $PbCO_3$ by XRD and Raman spectroscopy. Chinese Phys. C. 2013:37,38001.